ELSEVIER

Journal of Nuclear Materials 304 (2002) 189–203

journal of nuclear materials

www.elsevier.com/locate/jnucmat

Delayed hydride cracking in Zr–2.5Nb pressure tube material ☆

R.N. Singh [a,*], Niraj Kumar [b,1], R. Kishore [a], S. Roychaudhury [a], T.K. Sinha [a], B.P. Kashyap [c]

[a] *Materials Science Division, Bhabha Atomic Research Centre, Mumbai 400 085, India*
[b] *Heavy Water Board, Vikram Sarabhai Bhavan, Mumbai 400 094, India*
[c] *Department of Metallurgical Engineering and Materials Science, Indian Institute of Technology, Powai, Mumbai 400 076, India*

Received 28 January 2002; accepted 1 May 2002

Abstract

Delayed hydride cracking (DHC) is one of the localized forms of hydride embrittlement caused by hydrogen migration up the tensile stress gradient. In this work, DHC velocity was measured along the axial direction of the double melted, cold worked and stress-relieved zirconium–2.5niobium pressure tube material in the temperature range of 162–283 °C. The DHC crack growth was monitored using the direct current potential drop (DCPD) technique. The calibration curves between the normalized DCPD output and the normalized crack length at different test temperatures were also used to determine the DHC velocity. A simple model capable of explaining the observed features of DHC is proposed. The model explains the basis for the occurrence of incubation period associated with DHC crack initiation. Activation energy associated with the DHC in this alloy was found to be 56 kJ/mol.

1. Introduction

Cold worked and stress-relieved tubes made up of Zr–2.5 wt% Nb alloy serve as the pressure boundary for the hot coolant in pressurized heavy water reactors (PHWR) [1–5]. Though the initial hydrogen content of these tubes is kept as low as possible by controlling the manufacturing process parameters [6], it can pick up hydrogen/deuterium during service [7]. Hydrogen is reported to have deleterious influence on the integrity of the dilute zirconium alloy pressure tubes [5,7–20]. This is manifested as gross and localized embrittlement [21]. Gross embrittlement is caused by uniformly distributed hydride precipitate, and it requires certain minimum volume fraction of the embrittling phase (in this case zirconium hydride) for a measurable loss of ductility and fracture toughness [22]. The localized embrittlement is an insidious degradation mechanism in which very slow damage accumulation takes place within a very small region over a period of time before any catastrophic failure may occur. In Zr-alloys, localized embrittlement is caused by the migration of hydrogen up the tensile stress gradient and down the thermal gradient and is manifested as delayed hydride cracking and hydride blister formation respectively.

Delayed hydride cracking (DHC) is a form of localized hydride-embrittlement phenomenon, which in the presence of a tensile stress-field manifests itself as a sub-critical crack growth process. It is caused by hydrogen migration up the tensile stress gradient to the region of stress concentration [5,9–13]. Once the local

☆ Part of this work has been published as BARC Report no. BARC/2001/E/026.

* Corresponding author. Fax: +91-22 550 5239.
E-mail address: mms@apsara.barc.ernet.in (R.N. Singh).

[1] Shri Niraj Kumar was involved with this study as project trainee, Metallurgy, 44th batch of training school, BARC. Presently he is posted at Heavy Water Board, Vikram Sarabhai Bhavan, Mumbai 400 094, India.

0022-3115/02/$ - see front matter
PII: S0022-3115(02)00880-2

solid solubility is exceeded, brittle hydride platelets precipitate normal to the tensile stress. Growth of hydride precipitate continues till a hydride platelet of critical size is formed [18,19]. A hydride platelet of the critical size cracks under concentrated stress leading to the growth of the crack. This crack growth is delayed by the time required for hydrogen to reach the crack tip and form hydride platelet(s) of critical size. Hence this phenomenon is called DHC. DHC is a discontinuous crack growth process and is characterized by crack growth rate, which is called DHC velocity (V_{DHC}). Fig. 1 shows schematically the variation of V_{DHC} with stress intensity factor (SIF). This figure shows that there exists a threshold for SIF below which V_{DHC} is negligible and above this threshold, V_{DHC} is independent of the SIF. A second threshold corresponds to fracture toughness of the material above which the crack grows in an unstable manner [20].

The tubes for the Indian PHWRs are manufactured at Nuclear Fuel Complex, Hyderabad, following a fabrication route similar to the modified route II developed by Atomic Energy of Canada Limited (AECL) for the pressure tubes of CANDU reactors [23]. The modified route II [23] consists of two cold working steps (instead of one cold working step for the conventional route) and an intermediate annealing step. The lower extrusion ratio employed in the modified route compared to the conventional route ensures lower aspect ratio of α grains, less intense circumferential basal pole texture and more uniform microstructure resulting in improved irradiation resistance, reduced susceptibility to stress reorientation of hydrides, and uniform mechanical properties across the length of the tube [24]. Very little information is available in literature on the DHC behavior of this particular material [25,26]. The objective of this work was to determine the DHC velocity along the axial direction of the Zr–2.5Nb pressure tube alloy as a function of test temperature. The temperature ranges likely to be seen by the operating pressure tubes of PHWRs was the basis for selecting the test temperature range of 162–283 °C. The V_{DHC} was determined following the test procedure prescribed by IAEA for the round robin participants of a Coordinated Research Programme on 'Hydrogen and hydride induced degradation of physical and mechanical properties of zirconium alloys' [27]. The specimens prepared for IAEA round robin participants were electrolytically charged [28] while in the present study the specimens were gaseously charged with hydrogen [25,26]. The direct current potential drop (DCPD) technique [29] was used for crack-growth monitoring and DHC velocity estimation. A comparison of the DHC behavior results of Indian pressure tube material with those reported in the literature [5,9–13,20,30–32] is also presented.

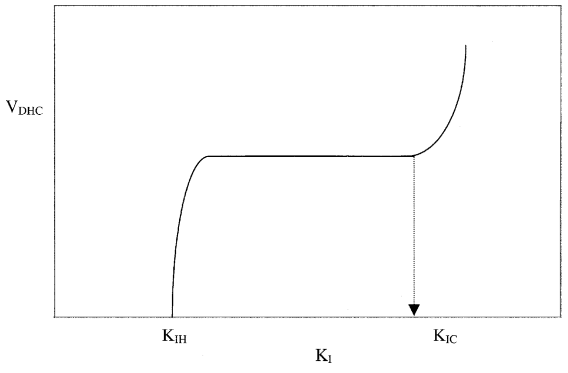

Fig. 1. Schematic showing the variation of DHC velocity (V_{DHC}) with SIF (K_I).

2. Experimental procedure

The materials used in this study were from double melted, autoclaved, unirradiated Zr–2.5Nb pressure tube (spool number 100-2-3) of PHWR 235 MWe. The dimensions of the tube were 81.5 mm diameter and wall thickness of 3.7 mm. The chemical composition of the Indian material used for this investigation is given in Table 1. The room temperature yield and ultimate tensile strength of the Indian material was 599 and 833 MPa respectively and the tensile elongation was 13.3% in a 25 mm gage length. The pressure tube sections of length 110 mm were polished up to 1200 grit emery paper to obtain oxide free surface and subsequently these tube sections were gaseously charged with 40 or 60 or 80 ppm by weight of hydrogen. Curved compact toughness (CCT) specimens of width 17 mm were machined from these spools. Ten CCT specimens, identified as 411 to 420, were provided to the Materials Science Division, BARC by AECL through IAEA under the CRP [27]. These specimens were machined from the section RX094-C2-4 of quadruple melted, unirradiated, finished autoclaved CANDU Zr–2.5Nb pressure tube.

Table 1
Chemical composition of the Indian pressure tube material (in % by weight) used in the present investigation

%Nb	O	H	N	Sn	Cr	Ni	Fe	Zr
2.53	0.1226	0.0010	0.0056	0.0180	0.020	<0.007	0.13	Balance

The specimens have been machined from the electrolytically hydrogen charged (to 63 ppm by weight) rings of Zr–2.5Nb pressure tube material [28].

Fatigue precracking was carried out using tapered pins to obtain a sharp and uniform crack tip. The SIF, K_I, was calculated using Eqs. (1) and (2) [27]:

$$K_I = \frac{P_Q}{BW^{1/2}} f(a/W), \tag{1}$$

where P_Q = applied load (N), B = specimen thickness (m), W = specimen width (m), a = crack length (m) and

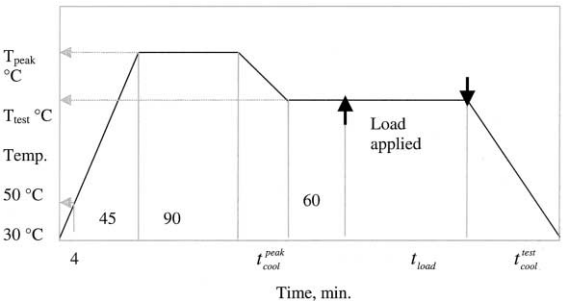

Fig. 2. Schematic shows the thermal cycle, to which specimen were subjected to during the DHC test.

$$f\left(\frac{a}{W}\right) = \frac{\left[2+\frac{a}{W}\right]\left[0.886+4.64\frac{a}{W}-13.32\left(\frac{a}{W}\right)^2+14.72\left(\frac{a}{W}\right)^3-5.6\left(\frac{a}{W}\right)^4\right]}{\left(1-\frac{a}{W}\right)^{3/2}}. \tag{2}$$

The DHC testing procedure recommended by IAEA [27] was followed in the present investigation. A SATEC creep testing machine was used to carry out DHC tests. The equipment consisted of single arm lever type loading system fitted with a resistance heated single zone furnace. The lever arm ratio of the loading system was 1:17. The specimens were subjected to a thermal cycle shown below and illustrated schematically in Fig. 2.

parentheses) is also shown in this table. The temperature of the testing furnace was controlled within 1 °C through a K-type thermocouple. A load of 15 lb (or 66.78 N AECL material)/12 lb (or 54.3 N Indian material) was placed on the lever pan quasi-statically once the specimen attained the test temperature. The DHC crack growth was monitored using a direct current potential drop technique [25,26,29]. The temperature of

$$30\ ^\circ\mathrm{C} \xrightarrow[4\ \mathrm{min}]{\mathrm{Heat}} 50\ ^\circ\mathrm{C} \xrightarrow[45\ \mathrm{min}]{\mathrm{Heat}} T_{\mathrm{peak}} \xrightarrow[90\ \mathrm{min}]{\mathrm{Soak}} T_{\mathrm{peak}} \xrightarrow[t_{\mathrm{cool}}^{\mathrm{peak}}\ \mathrm{min}]{\mathrm{Cool}} T_{\mathrm{test}} \xrightarrow[60\ \mathrm{min}]{\mathrm{Soak}} T_{\mathrm{test}} \xrightarrow[t_{\mathrm{load}}\ \mathrm{min}]{\mathrm{Load}} T_{\mathrm{test}} \xrightarrow[t_{\mathrm{cool}}^{\mathrm{test}}]{\mathrm{Unload,\ cool}} 30\ ^\circ\mathrm{C}$$

The test data including peak temperature, T_{peak}, and cooling time, t_{cool}^{peak}, from T_{peak} to test temperature, T_{test} for DHC tests carried out at different temperatures are given in Table 2. The amount of hydrogen charged and that estimated by inert gas fusion technique (in

the CCT specimens was monitored using K-type thermocouple (0.2 mm dia.) spot welded to the inside curvature of the CCT specimens within 1 mm of the fatigue precrack. This thermocouple was designated as spn. T/C1.

Table 2
Test details including peak temperature (T_{peak}) and cooling times (t_{cool}^{test}) from T_{peak} to test temperature (T_{test}) to which the specimens were subjected to during DHC tests

Test Id	T_{peak} °C	T_{test} °C	H content charged (estimated)	t_{cool}^{peak} S	t_{load} S	t_{cool}^{test} S
DHC26 to DHC28 DHC42	320	162	40 (55, 32)	9480	234 000 (65 h)	10 800
DHC35 to DHC37	320	182	40 (55, 32)	8280	172 800 (48 h)	9420
DHC38 DHC39	320	203	40 (55, 32)	7020	72 000 (20 h)	10 800
DHC32 to DHC34	320	227	60 (130, 69, 53, 45, 45)	5580	43 200 (12 h)	12 000
DHC04–06 & DHC40	320	250	60 (130, 69, 53, 45, 45)	4200	21 600 (6 h)	15 000
DHC07–10			80 (67, 36, 40)			
DHC11 to DHC20	315	250	63 (44, 43)	3900	21 600 (6 h)	15 000
DHC29 to DHC31	350	283	80 (67, 36, 40)	4020	10 800 (3 h)	15 000
DHC41	320	283		2220	10 800	15 000

Amount of hydrogen charged and that estimated from inert gas fusion technique (in parentheses) are also shown.

In order to measure the DHC crack and the fatigue precrack, the CCT specimens subjected to DHC testing were pulled apart into two halves. Before pulling the specimens apart, they were fatigue postcracked to delineate the DHC cracks properly. The DHC cracks '*D*' and fatigue precrack 'FPC' was measured directly from the specimen using a *XY*-microscope of resolution 0.5 μm. The fatigue precrack and DHC crack length were estimated as the average of nine equispaced readings [27]. For some specimens, one half of the broken CCT specimens were photographed using a Sony digital camera Mavica MVC-FD-95. The DHC crack was estimated from the fractograph as the average of nine equispaced readings [27]. The DHC crack was also measured from the DCPD output [25,26,29]. For tests conducted at a temperature lower than 250 °C, striations on the fracture surface were not clearly visible and hence a heat tinting treatment at 300 °C for half an hour was used.

3. DCPD technique for sub-critical crack growth monitoring

The electrical potential drop method [29] is one of the most commonly used techniques for measuring crack initiation and sub-critical crack growth at elevated temperatures. In this technique the increase in electrical resistivity of a specimen to which a constant current (ac or dc) is applied is used to monitor crack extension. The main advantages of the dc potential drop method are the comparatively simple test set-ups and the capability of the technique to derive a correlation between crack-length and potential drop in a certain type of specimen by means of either analytical or numerical calculations. By measuring DCPD output across standard specimens with known crack length and by plotting the normalized DCPD output against the crack length (*a*) or the normalized crack length, *a*/*W*, calibration curve can be generated. Similarly, by measuring the DCPD output as a function of temperature, the temperature dependence of the output voltage can be established. A combination of these two curves can be used for sub-critical crack growth monitoring [25]. The main features of the DCPD system used for crack growth monitoring in the present investigation are described below.

DCPD system consisted of a constant current unit to supply a constant dc current, an arrangement to supply this current through specimen, an arrangement to measure the potential drop across the notch/crack in the specimen and provision to record the DCPD output, temperature and current continuously. The current was supplied to the specimen through screw tightened copper lugs welded to copper wires. The DCPD output was measured using the wire of the same material (in this case Zr–2.5Nb) to avoid error due to thermocouple effect. For this purpose, 0.5 mm diameter Zr–2.5Nb wires were spot-welded to CCT specimen within 1 mm of the each side of the notch. A constant dc current was used for the DHC tests. The DCPD signal, specimen and furnace temperatures and current were continuously recorded on 12-channel videographic *XY* recorder.

4. Results

Fig. 3(a)–(c) shows the micrographs of the Zr–2.5Nb pressure tube specimens along the radial–circumferential plane. These specimens were charged with 40, 60 and 80 ppm of hydrogen by weight. The traces of circumferential hydrides (dark lines) can be seen in these micrographs. The microstructure and the texture of the pressure tube [5,24] are such that only circumferential hydrides form in the as-hydrided condition. A typical plot showing the variation of the temperature of the specimen and DCPD output is shown in Fig. 4. For all the tests the specimen temperatures remained constant throughout the DHC testing. The DCPD output was linear for the entire duration for which the specimen was under load, indicating that DHC crack propagation was uniform. The fatigue precrack and the DHC crack lengths were measured as nine-point average. A typical fractograph obtained in this test is shown in Fig. 5 for both the Indian and AECL material tested at 250 °C. Three regions viz. fatigue precrack, DHC crack and fatigue post crack can be seen clearly in this figure. The fracture surface of the Indian material was uneven and marked with fibrous feature parallel to the axial direction of the tube. Compared to this, the fracture appearance for the AECL material was smooth and much cleaner. This could be due to the lower impurity content in the quadruple melted AECL material compared to the double melted Indian material. DHC crack growth is a discontinuous process and hence the fracture surface is marked by striations. A typical photograph showing striations on the fracture surface is shown in Fig. 6.

The summary of the DHC tests carried out on double melted Indian pressure tube material is given in Table 3(panel A) and that for quadruple melted AECL material is given in Table 3(panel B). The DCPD output showed an incubation period for crack initiation for some of the tests (Table 3). The DHC velocity was determined for this material in the temperature range of 162–283 °C and the results are given in Table 4. It can be seen from Table 4 that with an increase in test temperature, the DHC velocity increases. Fig. 7 shows a plot of DHC velocity against the inverse of the test temperature. From slope of this plot the activation energy associated with delayed hydride cracking was determined and found to be about 56 kJ/mol.

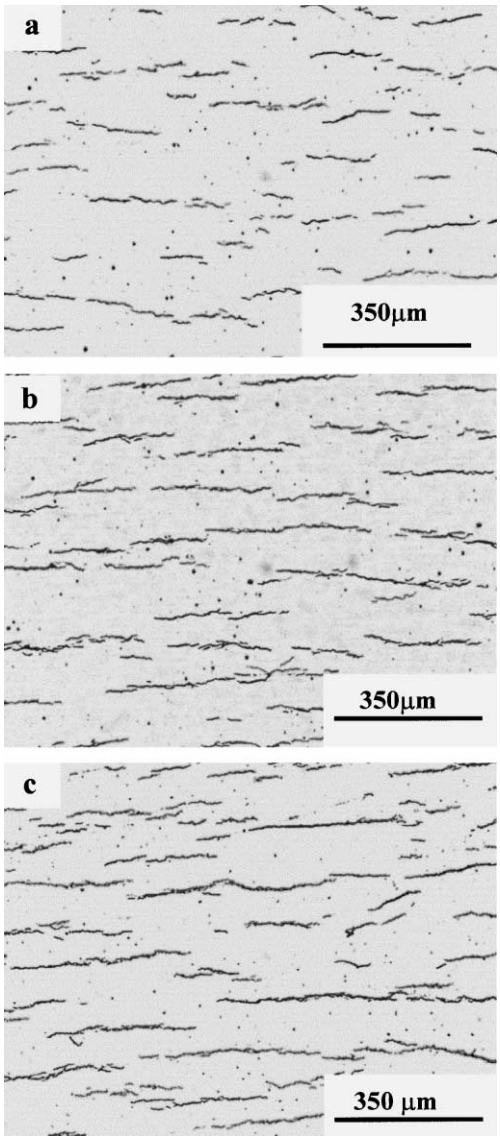

Fig. 3. Micrograph of as-hydrided material showing hydride morphology and distribution for Zr–2.5Nb pressure tube material containing (a) 40 ppm, (b) 60 ppm and (c) 80 ppm of hydrogen by weight for radial–circumferential plane of the pressure tube. Traces of hydrides (dark lines) can be seen.

4.1. Crack length estimation from DCPD

DCPD output in the present investigation was a function of crack length and temperature. Fig. 8(a) shows the variation of DCPD output with normalized crack length at ambient temperature. This plot is linear with a/W in the range of 0.4 to 0.7. A linear regression analysis suggested a relationship between normalized DCPD output and normalized crack length of the form

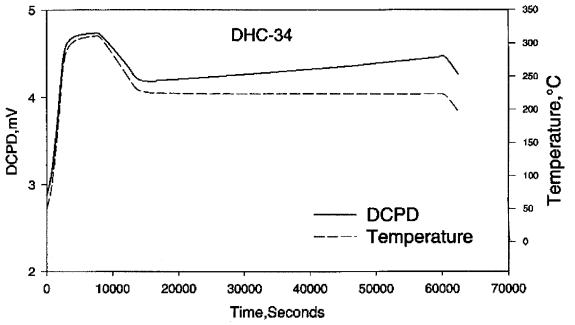

Fig. 4. Plot of DCPD and specimen temperature against time obtained during DHC test carried out at 227 °C.

represented by Eq. (3). This equation can be used to monitor crack growth online during fatigue precracking.

$$V/V_0 = 0.565 + 1.084(a/W). \tag{3}$$

For calibration with respect to temperature, the test temperature was approached from the higher side. Fig. 8(b) shows the variation of normalized DCPD output with temperature for a fixed crack length. The variation of DCPD with temperature was linear but the slope of the DCPD versus temperature plots increased gradually with increasing crack length. Thus it was not possible to use a single calibration curve for obtaining the crack length from the DCPD and corresponding temperature value. However, it was observed that the slope of the DCPD temperature plot was constant for small change in crack length. The procedure for estimating the crack length is outlined below.

Let the DCPD output at room temperature for a fixed current be V_0 and V_F^{RT} corresponding to a crack length of a_0 (crack length obtained by machining), and a_F (crack length obtained after fatigue precracking) respectively. From Eq. (3), using the ratio V_F^{RT}/V_0 the value of a_F can be obtained. The values of a_F obtained from DCPD values for some of the tests are compared in Table 5 with the crack length measured directly using a XY microscope. As can be seen, the values are quite close.

For a given crack length the variation of normalized DCPD output with temperature was linear. Thus, normalized DCPD output can be expressed as

$$V/V_0 = c + d(T - 273) \quad T \text{ in K}. \tag{4}$$

In Eq. (4), the intercept c is a strong function of crack length while slope d is a very weak function of crack length. Both c and d change with variations in the nature and location of contact. Unless proper precautions are taken, the crack length obtained from the DCPD measurements could be in error. A method for estimating the crack length from the DCPD outputs obtained during the DHC test is proposed as follows.

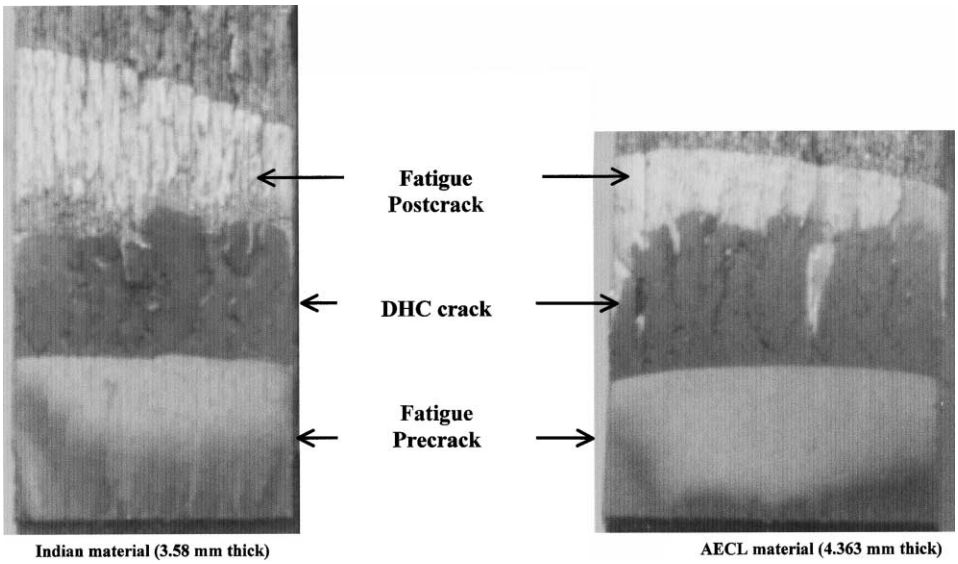

Fig. 5. Fractograph showing the fatigue precrack (FPC), DHC crack (D) and fatigue post crack for CCT specimens subjected to DHC testing at 250 °C.

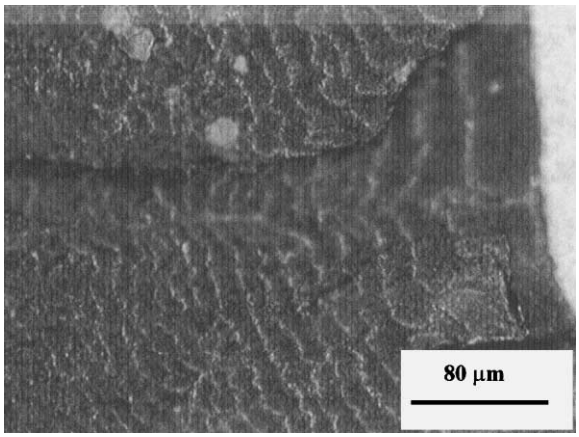

Fig. 6. A typical photograph of fracture surface showing striations. These striations indicate the discontinuous nature of DHC crack propagation.

Let the DCPD output at the test temperature be V_F^{Test} and V_D^{Test} corresponding to a crack length of a_F and a_D (crack length obtained at the end of DHC) respectively. The crack length can be obtained from Eq. (3) if V_D^{RT}/V_0 is known. In order to estimate V_D^{RT}/V_0, the value of intercept c and slope d is required. The value of c and d can be obtained using Eqs. (5) and (6). Knowing c and d, the ratio V_D^{RT}/V_0 can be estimated using Eq. (7).

$$\frac{V_F^{Test}}{V_0} = \frac{V_F^{RT}}{V_0} + d(T^{Test} - T^{RT}), \tag{5}$$

$$\frac{V_D^{Test}}{V_0} = c + d(T^{Test} - 273), \tag{6}$$

$$\frac{V_D^{RT}}{V_0} = c + d(T^{RT} - 273), \tag{7}$$

where, V_D^{RT} is the DCPD output at room temperature and T^{Test} and T^{RT} are the test and room temperatures in K respectively. The DHC crack length estimated following this procedure is given in Table 6. The crack length values obtained from DCPD and direct measurement under a XY microscope are also compared in this table. The crack length values (a_D) obtained by DCPD are within ±4% of the crack length directly measured under the microscope. A comparison of the V_{DHC} estimated from DCPD output and by direct measurement under XY microscope for selected tests is shown in Table 7(panel A). For some specimens the DHC crack length (D) was measured from the photograph of the fracture surface at a magnification of six times. The V_{DHC} estimated from fractography, DCPD and XY microscope are compared for selected specimens in Table 7(panel B).

5. Discussion

It is believed that DHC crack growth involves hydrogen migration [5], hydride nuclei reorientation [33], growth of the hydride nuclei to critical size [18,19] and crack propagation. First the hydrogen concentration

Table 3
Summary of selected DHC tests for DHC velocity (V_{DHC}) measurement along the axial direction of the double melted Zr–2.5Nb pressure tube alloy (Indian material) (Panel A) and summary of DHC test results for DHC velocity (V_{DHC}) measurement along the axial direction of the quadruple melted Zr–2.5Nb alloy (specimens supplied by IAEA–AECL material) (Panel B)

Panel A

Test no./ spn. id	H conc. (wt ppm)	Temperature (°C)		Crack length (mm)			Time (s)		V_{DHC} ($\times 10^{-8}$ m/s)	Load (kg)	K_I (MPa m$^{1/2}$)	
		Peak	Test	Notch, *a*	FPC	D	Incubation	Cracking			Initial	Final
DHC04A10	60	345	257	6.790	3.8600	0.6655	Nil	7800	8.53	84.82	24.62	29.20
DHC05A1	60	325	253	6.570	3.1600	1.2524	Nil	13 560	9.24	84.82	16.65	20.71
DHC06A2	60	319	257	6.650	3.2800	0.7736	Nil	9600	8.06	84.82	16.97	19.34
DHC25A3	60	314	203	6.675	2.3741	1.3863	Nil	72 000	1.92	92.53	18.80	25.35
DHC21A5	60	315	203	6.700	3.2316	1.8674	Nil	72 000	2.59	92.53	22.20	35.50
DHC23A9	60	314	203	6.755	4.6192	1.1134	Nil	49 380	2.25	57.83	20.26	28.80
DHC24A11	60	314	203	6.810	3.0095	1.1694	Nil	72 000	1.62	92.53	23.03	29.05
DHC26C10	40	320	162	6.743	2.1522	1.2671	9230	224 740	0.5638	92.53	20.218	25.936
DHC27C12	40	320	162	6.723	2.3021	1.7900	9260	224 630	0.7968	92.53	20.622	30.710
DHC28C09	40	320	162	6.765	1.8410	1.0609	8650	225 350	0.471	92.53	19.121	23.490
DHC30D10	80	350	283	6.820	0.9237	1.8344	0	11 290	16.248	92.53	16.370	23.493
DHC31D11	80	350	283	6.798	1.8074	1.6893	0	9570	17.65	92.53	19.114	27.156
DHC32A16	60	320	227	6.645	1.6466	1.8182	310	43 060	4.208	92.53	18.150	25.991
DHC33A18	60	320	227	6.640	0.9868	1.9525	0	43 800	4.4577	92.53	16.096	23.517
DHC34A21	60	320	227	6.765	2.2975	1.5307	0	43 470	3.521	92.53	20.622	29.208
DHC35C06	40	320	182	6.695	2.7079	1.6202	4410	168 130	0.9636	92.53	24.279	32.335
DHC36C07	40	320	182	6.713	2.5006	1.5758	9250	162 580	0.9692	92.53	24.281	30.701
DHC37C08	40	320	182	6.860	3.0383	1.7360	6000	166 200	1.044	92.53	25.368	38.243
DHC38C03	40	320	203	6.725	1.7940	1.3580	6340	65 890	2.061	92.53	18.765	25.349
DHC39C04	40	320	203	6.665	2.8244	1.3577	0	71 520	1.898	92.53	23.493	30.699
DHC40A19	60	320	250	6.700	2.0503	1.6960	0	20 670	8.205	92.53	19.861	28.517
DHC41D12	80	320	283	6.663	2.4438	0.5780	0	10 420	5.547	92.53	20.622	23.498

Panel B

Test no./spn. id	H conc. (wt ppm)	Temperature (°C)		DHC crack length (mm)	Time (min)		DHC (vel. $\times$ 10^8 m/s)	K_I (MPa m$^{1/2}$)	
		Peak	Test		Incubation	Cracking		Initial	Final
DHC11/411	63	304/305	248	1.4415	Nil	360	8.14	18.94	27.10
DHC12/412	63	304/305	248	1.5955	Nil	355	7.87	18.92	26.51
DHC13/413	63	304/305	248	1.5819	Nil	362	7.665	18.59	25.94
DHC14/414	63	304/305	246	1.7456	Nil	358.5	9.10	19.15	28.52
DHC15/415	63	304/305	245	1.5835	Nil	357.33	8.90	19.96	29.85
DHC16/416	63	304/305	246	1.6918	Nil	358.33	8.46	18.74	26.96
DHC17/417	63	304/305	246	1.5410	Nil	359	7.98	19.04	26.81
DHC18/418	63	304/305	248	1.6882	Nil	358	8.50	20.27	29.65
DHC19/419	63	304/305	246	1.8464	Nil	360	7.75	19.3	27.31
DHC20/420	63	304/305	245	1.4653	Nil	358	7.49	19.98	27.97

builds up in a region near the crack tip and once the local terminal solid solubility limit is exceeded, hydride nucleation occurs. During DHC, the hydride nuclei precipitate perpendicular to the stress axis [9–13,33] i.e. along the radial-axial plane, for specimens subjected to tensile stress along the circumferential direction of the tube. Once the hydride precipitate of critical size forms [18] it cracks resulting in slow crack growth and the whole sequence repeats. Thus DHC is a time dependent discontinuous crack growth process consisting of formation of hydride precipitate of critical size and cracking [5]. Each crack growth step is delayed by the time required for the precipitation of the hydride of critical size [18,19]. This gives rise to the appearance of striations on the fracture surface of the DHC tested specimens [30]. Such striations on the fracture surface are shown in Fig. 6 for a typical DHC test carried out in the present investigation.

Table 4
The variation of DHC velocity (V_{DHC}) for Indian material (Table 3(panel A)) in the temperature range of 162–283 °C

Test temperature (°C)	Test Id	H-content (wt ppm)	V_{DHC}	$V_{DHC(avg)}$
162	DHC 26	40	0.5638	0.6105
	DHC 27	40	0.7968	
	DHC 28	40	0.471	
182	DHC 35	40	0.9636	0.9922
	DHC 36	40	0.9692	
	DHC 37	40	1.0440	
203	DHC 21	60	2.59	2.0565
	DHC 23	60	2.25	
	DHC 24	60	1.62	
	DHC 25	60	1.92	
	DHC 38	40	2.061	
	DHC 39	40	1.898	
227	DHC 32	60	4.208	4.0622
	DHC 33	60	4.4577	
	DHC 34	60	3.5210	
250	DHC 04	60	8.53	7.6069
	DHC 05	60	9.24	
	DHC 06	60	8.06	
	DHC 07	80	7.15	
	DHC 08	80	6.32	
	DHC 09	80	6.60	
	DHC 10	80	6.75	
	DHC 40	60	8.205	
283	DHC 29	80	–	16.949
	DHC 30	80	16.248	
	DHC 31	80	17.65	

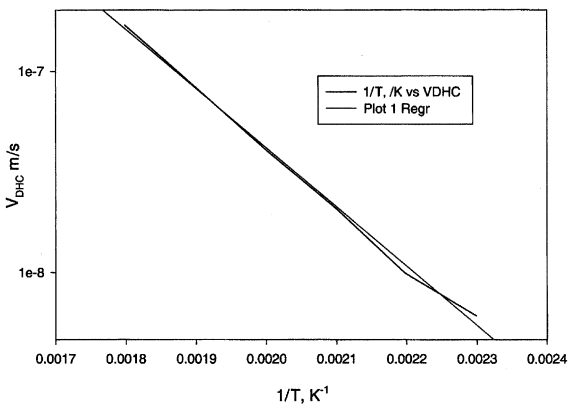

Fig. 7. Plot of DHC velocity (V_{DHC}) vs. inverse of test temperature.

A summary of the experimental observations reported on DHC in the literature [5,9–13,18–20,30–32] is as follows:

1. DHC crack initiation is associated with an incubation period.
2. DHC crack initiation is associated with a threshold SIF, K_{IH}, below which DHC crack growth velocity, V_{DHC} is immeasurable.
3. K_{IH} is practically independent of material strength.
4. For a given material and for $K_{IH} < K_I < K_{IC}$ (fracture toughness of the material), V_{DHC} is independent of applied stress intensity factor, K_I.
5. V_{DHC} increases with increase in strength of the material.

Some of the observations listed above are only qualitatively understood. A simple model of DHC capable of providing the basis for quantification of the above observations is proposed in Section 5.1.

5.1. DHC model

The region ahead of the crack tip for an elasto-plastic material [34] (like zirconium alloys) reveals that it can be divided into three zones. These are the process zone (stress $\geqslant \sigma_0$, yield strength of the material), a reorientation zone experiencing elastic stress greater than σ_{th}, (threshold stress for reorientation of hydrides) and a migration zone experiencing stress lower than σ_{th}. This is illustrated schematically in Fig. 9(a). Fig. 9(b) shows schematically the variation in stress gradient in the process, reorientation and migration zones. The diffusion equation in one dimension [5] for hydrogen migration under concentration, temperature and stress gradient is as follows:

$$J = \frac{-DC_r}{RT}\left[RT\frac{\mathrm{d}\ln C_r}{\mathrm{d}r} + \frac{Q^*}{T}\frac{\mathrm{d}T}{\mathrm{d}r} - \frac{V^*}{3}\frac{\mathrm{d}\sigma}{\mathrm{d}r}\right], \tag{8}$$

where, C_r is the hydrogen concentration at any point at a distance r, D the diffusivity of hydrogen in metal, J the hydrogen flux, Q^* the heat of transport of hydrogen in metal, R the gas constant, T the temperature, V^* the volume of transport of hydrogen in metals, σ the tensile (taken +ve) or compressive (taken as −ve) stress. Eq. (8) suggests that the driving force for hydrogen migration during DHC is the stress gradient, which is a maximum in the reorientation zone and a minimum in the process zone. Thus in terms of the three zones identified ahead of the crack tip, each DHC crack growth step comprises of four processes. These are:

1. Hydrogen migration up the tensile stress gradient in the reorientation zone.
2. Precipitation of brittle hydride in the reorientation zone.
3. Growth of the hydride in the reorientation zone to a critical size and

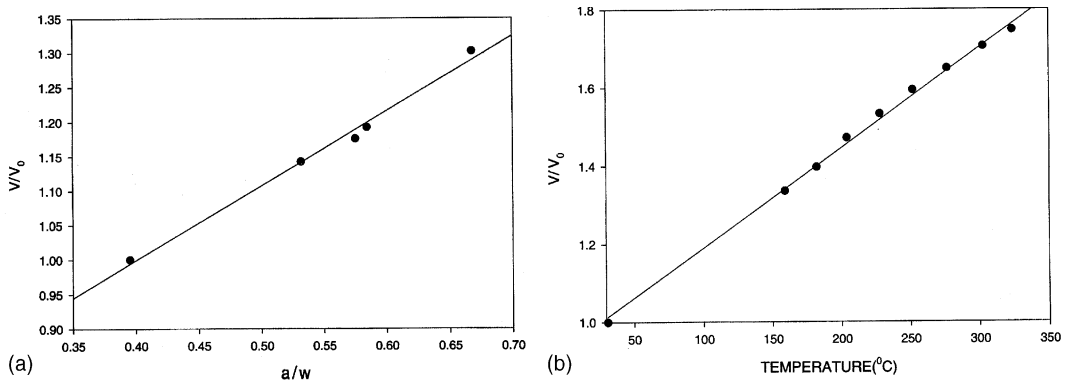

Fig. 8. The variation of normalized DCPD output with (a) normalized crack-length at ambient temperature and (b) temperature for a fixed crack length.

Table 5
The values of crack length obtained after fatigue precracking (a_F) estimated from DCPD values for some of the tests are compared with the values measured using XY microscope. As can be seen, the values of FPC obtained from both the methods are similar

Test no	V_0	V_F^{RT}	V_F^{RT}/V_0	a_F/W DCPD	a_F DCPD	FPC	
						DCPD	XY
DHC 28	2.345	2.61	1.113	0.5055	8.601	1.8360	1.8410
DHC 30	1.024	1.084	1.058	0.4548	7.736	0.9160	0.9236
DHC 31	2.337	2.601	1.113	0.5055	8.607	1.8095	1.8074
DHC 32	2.438	2.670	1.095	0.4889	8.287	1.642	1.6466
DHC 33	2.458	2.586	1.052	0.4492	7.625	0.9850	0.9868
DHC 35	2.424	2.822	1.164	0.5525	9.401	2.7060	2.7079
DHC 36	2.443	2.814	1.152	0.5415	9.212	2.4995	2.5006
DHC 37	2.407	2.878	1.196	0.5821	9.902	3.0420	3.0383
DHC 38	2.541	2.813	1.107	0.5000	8.517	1.7920	1.794
DHC 39	2.426	2.837	1.169	0.5571	9.479	2.8140	2.8244
DHC 40	2.730	3.067	1.123	0.5147	8.742	2.0420	2.0503

4. Crack growth by cracking of hydride of critical size in reorientation zone leading to the rupture of the process zone.

Since the cracking of the hydride and the rupture of the process zone are delayed by the time required for the formation of hydride precipitate of critical size in the reorientation zone (which experiences maximum stress gradient – the driving force for hydrogen migration) this phenomena is called DHC.

5.2. Incubation period for DHC

Usually DHC is reported to be associated with an incubation period for crack initiation [20]. However, the understanding of the incubation period is still qualitative [20]. DHC is a discontinuous crack growth process. As explained above, a single crack growth step involves diffusion of hydrogen, precipitation of hydride and cracking of the hydride and the process zone ahead of the crack tip. Distinction has to be made between the first and the subsequent crack growth steps. The incubation period is the difference between the time period for the first and the subsequent crack growth step. The time period for a crack growth step during DHC will depend on hydrogen flux into the region ahead of crack tip and the susceptibility of process zone to hydrogen/hydride induced embrittlement. It is believed that the hydrogen flux for the subsequent crack growth step is greater than that for first crack growth. The factors affecting hydrogen flux are the test temperature [5], the stress gradient prevailing ahead of the crack tip [5] and uni- or bi-directional nature of the flux. As the test temperature during DHC testing is maintained constant, the possible causes of the occurrence of incubation period are:

1. Change in stress gradient due to variation in crack tip radius before and after the first crack growth step.

Table 6
DHC crack length estimated from DCPD values and comparison with the values measured using XY microscope. The values of the crack growth obtained during DHC (D) are given in last column

Test no	V_F^{Test} (mV)	V_F^{Test}/V_0	$d^{Test} \times 10^3$	V_{DHC}^{Test} (mV)	V_{DHC}^{Test}/V_0	C^{RT}	V_{DHC}^{RT}/V_0	a_D/W DCPD	a_D (mm) DCPD	D (mm) DCPD	D (mm) XY
DHC 28	3.600	1.535	3.109	3.74	1.595	1.091	1.168	0.556	9.460	0.8590	1.0609
DHC 30	2.449	2.392	5.221	2.714	2.650	1.172	.313	0.690	11.736	4.0000	1.8344
DHC 31	4.460	1.908	3.106	4.743	2.029	1.150	.235	0.618	10.522	1.9150	1.6893
DHC 32	4.096	1.680	3.128	4.413	1.810	1.099	.213	0.597	10.119	1.832	1.8122
DHC 33	3.962	1.612	2.923	4.256	1.731	1.067	.183	0.570	9.675	2.0500	1.9525
DHC 35	4.060	1.675	3.351	4.277	1.764	1.154	.257	0.638	10.855	1.4540	1.6202
DHC 36	3.966	1.623	3.246	4.164	1.704	1.113	.233	0.616	10.479	1.2670	1.5758
DHC 37	4.084	1.697	3.238	4.370	1.816	1.226	.307	0.684	11.635	1.7330	1.7360
DHC 38	3.994	1.572	3.027	4.150	1.633	1.018	.169	0.557	9.488	0.971	1.358
DHC 39	4.211	1.736	3.279	4.399	1.813	1.148	.258	0.639	10.872	1.3930	1.3577
DHC 40	4.320	1.582	2.844	4.612	1.689	0.978	1.231	0.614	10.428	1.6860	1.6960

Table 7
Comparison of DHC velocity estimated by DCPD method and by direct measurement using a XY microscope (panel A) and comparison of DHC velocity 10^{-8} m/s calculated from crack lengths measured by different methods (panel B)

Test no	Test temperature (°C)	$V_{DHC} \times 10^8$(m/s) DCPD	XY	
Panel A				
DHC 28	162	0.3769	0.4655	
DHC 35	182	0.8648	0.9636	
DHC 36	182	0.7793	0.9692	
DHC 37	182	1.0427	1.044	
DHC 38	203	1.4736	2.061	
DHC 39	203	1.9477	1.898	
DHC 32	227	4.2545	4.208	
DHC 33	227	4.6803	4.4577	
DHC 40	250	8.1567	8.205	
DHC 30	283	35.429	16.248	
DHC 31	283	20.010	17.650	
Panel B				
Spn. id	Test temperature (°C)	Fractograph (~6 X)	XY microscope	DCPD
411	248	8.14	6.67	7.03
412	248	7.87	7.48	6.18
413	248	7.665	7.28	6.25
414	246	9.10	8.10	6.98
415	245	8.90	7.38	5.42
416	246	8.46	7.86	7.71
417	246	7.98	7.15	6.31
418	248	8.50	7.86	6.12
419	246	7.75	8.54	7.89
420	245	7.49	6.82	7.49
Dl	248	7.54	7.15	5.64
D3	248	6.71	6.60	5.43
D4	248	7.07	6.75	5.39

2. Increase in the average hydrogen concentration of the process zone prevailing ahead of the crack tip before and after the first crack growth step.
3. Enhancement of the susceptibility of the process zone to the hydrogen/hydride induced embrittlement before and after the first crack growth step and
4. Difference in hydrogen flux into the region ahead of the crack tip before and after the first crack growth step.

Thus, the corresponding components of the incubation period can be written as

$$t_{incubation} = t_{cracktip} + t_{migration} + t_{hydrogenembrittlement} + t_{doubleflux}. \quad (9)$$

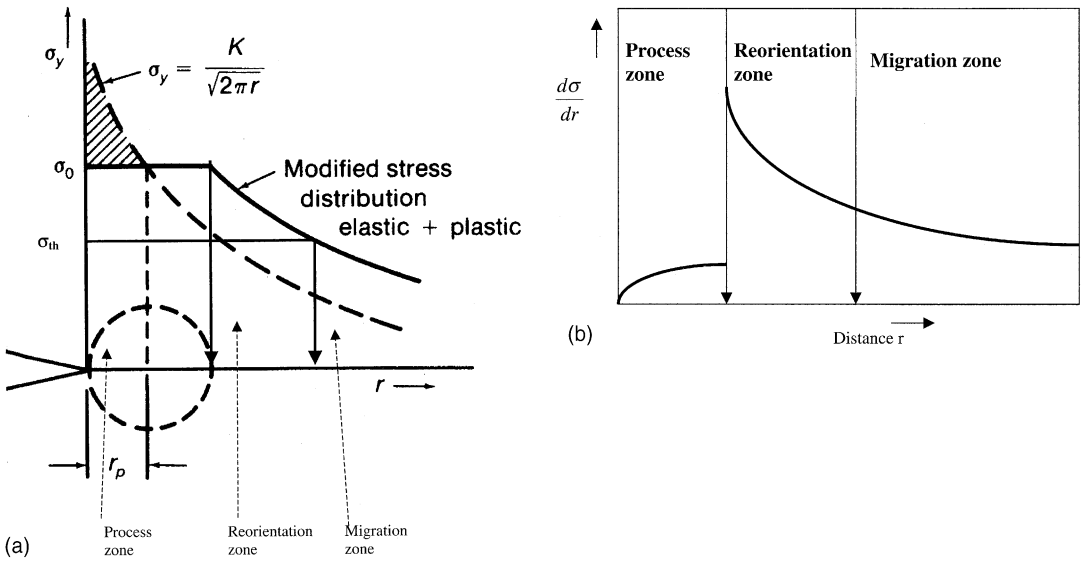

Fig. 9. (a) Schematic showing three zones ahead of crack tip. In the process zone, the stress is greater than the yield strength of the alloy, in the reorientation zone the stress is more than the threshold stress of reorientation of hydrides in the alloy and in the migration zone the stress is less than the threshold stress for reorientation of hydrides but stress gradient is sufficient to cause thermal migration of hydrogen. (b) Schematic showing the variation of the stress gradient in different zones ahead of the crack tip. The stress gradient, which is the driving force for hydrogen migration, is maximum in the reorientation zone.

The crack tip radius governs the stress gradient prevailing ahead of the crack [34] and for a given temperature, the stress gradient is the driving force for hydrogen migration [5]. If the crack tip radius obtained by fatigue precracking is of the order of that obtained by hydride platelet cracking, component of the incubation period required for transforming a blunt crack into a sharp crack (t_{cracktip}) will diminish. In order to obtain a sharp crack, one has to ensure that during final stage of fatigue precracking, the SIF is low enough to prevent plastic deformation at the crack tip.

The stress field prevailing ahead of the crack tip influences the local equilibrium solid solubility for hydrogen [12] and provides the driving force for hydrogen migration towards the crack tip. It is clear from Fig. 9(b) that the maximum driving force (stress gradient) for hydrogen migration exists in the reorientation zone while the minimum driving force exists (Eq. (8)) in the process zone. Initially, hydrogen migration takes place from the bulk to the reorientation zone through migration zone. Once the local solid solubility is exceeded in the reorientation zone, hydrides precipitate normal to the stress. After attaining a critical size, both the process zone and the reorientation zone fractures apart under the concentrated stress leading to crack propagation. As a result of crack propagation, part of the migration zone becomes process and reorientation zone and the whole process of hydrogen migration, precipitation and crack propagation repeats. Since the subsequent process zones form in the migration zone, they are expected to contain a higher amount of hydrogen than the first process zone.

Let the bulk hydrogen concentration be C_0, the average hydrogen concentration in the reorientation zone at the end of the first DHC step be C_{R}^{σ}, and the average hydrogen concentration in the migration zone at the end of first cracking step be C_{M}^{σ}. Obviously, one would expect $C_0 < C_{\text{M}}^{\sigma} < C_{\text{R}}^{\sigma}$. For the first cracking step the delay time will be the time required to change the average concentration of reorientation zone from C_0 to C_{R}^{σ}. However, for subsequent DHC steps, the delay time will be the time required to change the hydrogen concentration from C_{M}^{σ} to C_{R}^{σ}. The difference between these two time periods is the second component of incubation period (represented as $t_{\text{migration}}$ in Eq. (9)). It should be possible to compute theoretically this component of incubation period from the terminal solid solubility data [35], its dependence on stress [36] and estimation of the process and reorientation zone size defined in Fig. 9(a).

Also, compared to first process zone, subsequent process zones will have a higher hydrogen concentration. As is well known that hydrogen embrittles the metal matrix, the subsequent process zones will be more susceptible to hydrogen/hydride induced embrittlement. As a result of this, the critical size of hydrides required in the reorientation zone to cause the rupture of first process zone is expected to be greater than that for subsequent process zones. As a consequence of this, time required for first crack growth step should be greater

than that for subsequent crack growth steps. This is the basis for the third component of incubation period for DHC crack initiation (represented by $t_{\text{hydrogenembrittlement}}$ in Eq. (9)).

Compared to first DHC crack growth step, for the subsequent steps the hydrides cracked in the preceding reorientation zone, being stress free, can act as a source for hydrogen migration to the subsequent reorientation zones. Thus for subsequent crack growth steps, the bi-directional nature of hydrogen migration into the reorientation zone from the corresponding migration zone and the preceding reorientation zones will ensure a greater hydrogen flux compared to first crack growth step. This will ensure the formation of hydride precipitate of critical size within a shorter time. This is the basis for the fourth component of the incubation period (represented as $t_{\text{doubleflux}}$ in Eq. (9)).

The last three terms of the Eq. (9) can be computed theoretically and are unlikely to show large scatter in their values. However, the first term will depend upon the sharpness of the crack. The crack tip geometry used for DHC studies by different investigators varies from saw cut or machined notch [9] to sharp crack tip obtained by fatigue precracking [20,25,30–32]. Hence the incubation period is expected to vary depending upon the sharpness of the crack tip and is the reason for the large scatter observed in the incubation period reported by different investigators [9,20,25,30–32]. The incubation period for initiation of DHC at 250 °C for tests carried out under comparable initial SIF is reported to vary from a few minutes [31,32] to 360 min [30]. In these investigations [30–32], the specimens having constant hydrogen concentration were fatigue precracked and tested at nearly the same temperatures. It is suggested that the variations reported in Refs. [30–32] on the magnitude of incubation time for DHC crack growth are mainly due to the variation in the crack tip radius obtained during fatigue precracking. The role of temperature is to influence the hydrogen diffusivity. At higher temperatures, the hydrogen diffusivity is higher and hence a hydride platelet of critical size will be formed quickly. Thus at higher temperatures, a shorter incubation period is expected. This can be seen from Table 3(panel A).

5.3. Threshold stress intensity factor

The schematic in Fig. 1 shows the variation of DHC velocity with SIF. For a given temperature there exists a minimum SIF, K_{IH}, below which cracks cannot propagate by DHC [20]. This is called threshold stress intensity factor. Threshold stress intensity factor must provide:

1. A critical stress gradient to initiate hydrogen migration in the reorientation and migration zone (defined in Fig. 9).
2. Sufficient stress to cause the reorientation of the hydrides in the reorientation zone.
3. Sufficient stress to fracture the reoriented hydride of critical size formed in the reorientation zone and
4. Sufficient stress to rupture the matrix in the process zone ahead of the crack tip.

For each of these four steps of DHC, there exists a critical SIF value. The K_{IH} corresponds to the maximum critical SIF associated with any of these steps. Let us examine the relative significance of SIF required for these four steps of DHC.

SIF provides the stress gradient, which is the driving force for hydrogen migration into the region ahead of crack tip. From the diffusion Eq. (8) [5], it is obvious that for a given hydrogen concentration and temperature, there must exist a critical stress gradient below which no net migration of hydrogen will take place. Since for most of the dilute zirconium alloys (Zircaloy-2, Zircaloy-4, Zr–1%Nb and Zr–2.5%Nb) used in the nuclear industry, the continuum phase is the α-phase, the critical stress gradient and hence the critical SIF required for hydrogen migration should remain the same. The nature of the stress field ahead of the crack tip (Fig. 9) is such that there must exist a region (called the reorientation zone) ahead of the process zone for which the stress endured by the material will be more than the threshold stress for reorientation of hydrides in these alloys. Also, the fracture toughness of the hydrides (1–3 MPa $\sqrt{\text{m}}$ [5]) is much lower than the reported K_{IH} (5–10 MPa $\sqrt{\text{m}}$ [2]) in these alloys and hence the SIF associated with reorientation of hydride and its cracking should be of lowest magnitude. The stress intensity required to rupture the process zone will depend on the hydride precipitate size in the reorientation zone. For a given process zone size, a critical size of hydride exists for which the process zone will rupture. In other words, once the critical SIF for hydrogen migration is attained, the process zone is going to rupture. For a process zone of larger size, hydride of a larger size will be required and vice-versa. Thus threshold SIF for DHC initiation should correspond to SIF ensuring the critical stress gradient for hydrogen migration. As a result of this, the K_{IH} for all the dilute zirconium alloys should be nearly equal, which actually is the case [2]. This explains the reason for the occurrence of threshold SIF for initiation of DHC.

5.4. Stress intensity factor and V_{DHC}

With an increase in SIF for an elastic–plastic material, the process zone size will increase and the reorientation and the migration zones are merely shifted. One of the consequences of this is that the stress gradient in the reorientation and the migration zones remains un-

changed. Since the stress gradient controls the hydrogen flux [5], the hydrogen flux into the reorientation zone remains unchanged even with increased SIF. As a result of this the DHC velocity, which is strongly influenced by the hydrogen flux into the reorientation zone, remains unchanged with increase in SIF. Once the critical SIF, K_{IC}, is attained, crack growth becomes unstable and the crack grows spontaneously. This gives a second threshold SIF corresponding to the fracture toughness of the material.

In the present investigation, the DHC tests were performed in the temperature range of 162–283 °C, under a constant load corresponding to an initial K_I of ~16–25 MPa $\sqrt{m}$. As the crack length increased because of DHC crack growth, the K_I value also increased. It may be noted (from Table 3) that although the K_I value increased from about 19–38 MPa $\sqrt{m}$, the average DHC velocity remained constant within experimental error. The constant slope of the DCPD output versus time plot (Fig. 4) in the region of the DHC crack growth also suggested that the DHC velocity was independent of the variation in the average SIF. Also, from the fractographs it appeared that for some specimens the fatigue precrack front was not uniform through the thickness. This means that K_I varied correspondingly across the thickness as well. The fractograph showed the DHC crack front was parallel to the fatigue precrack front. This can happen only if the DHC crack grows at a constant rate, independent of K_I so long as K_I is greater than K_{IH} but less than K_{IC} of the material.

5.5. DHC velocity variation with temperature

The yield strength of this alloy decreases with increase in test temperature [37]. Since in the present investigation all the DHC tests were performed with nearly constant initial K_I, with an increase in the test temperature, the process zone size is expected to increase. However, as discussed in Section 5.4, the process zone size also increases with increase in K_I. But, so long as the stress gradient is sufficient to allow hydrogen migration into the reorientation zone, V_{DHC} remains unchanged. Also, at higher temperatures, not only the amount of hydrogen in solution is higher, the kinetics of hydrogen migration are faster resulting in a higher hydrogen flux. Thus due to increased hydrogen diffusivity, V_{DHC} is expected to increase. The influence of test temperature on V_{DHC} through increased hydrogen diffusivity at higher temperature is expected to dominate over that of increased process zone size because of deceasing strength with increase in test temperature. Fig. 7 shows the variation of DHC velocity with inverse of test temperature. As expected V_{DHC} increases with increase in test temperature. The observed higher velocity at higher temperature as compared to that at lower temperature is due to greater hydrogen flux at high temperature [18,19].

5.6. Comparison of V_{DHC} estimated by different methods

The crack lengths were estimated by three different methods. These were nine-point average method from fractograph (at a magnification of ~6) [27], nine-point average method by XY microscope (of resolution 0.5 μm) [25,26] and those calculated from DCPD calibration curves [25]. Table 7 compares the DHC velocity estimated by these methods. As can be seen, the values are within the limits of experimental error. For instance, the average values of V_{DHC} at 250 °C were 8.2×10^{-8} m/s (fractograph at ~6 X), 7.52×10^{-8} m/s (XY microscope) and 6.13×10^{-8} m/s (DCPD calibration curves) and the average values of V_{DHC} at 203 °C were 2.0565×10^{-8} m/s (XY microscope) and 2.12×10^{-8} m/s s (DCPD calibration curves). At lower temperatures, the V_{DHC} values estimated by DCPD were lower than those measured directly under XY microscope. However, at 283 °C the values estimated from DCPD were higher that those obtained by direct measurement under XY microscope (Table 7(panel A)).

5.7. Activation energy of DHC

Fig. 7 shows a plot of V_{DHC} vs. the inverse of the test temperature. The variation of V_{DHC} with temperature is reported to exhibit an Arrhenius type relationship [38]. Thus from the slope of the V_{DHC} versus inverse of test temperature plot, the activation energy associated with DHC can be determined. In the present investigation linear regression analysis yielded

$$V_{DHC} = \frac{da}{dt} = 0.031 \exp\left(\frac{-56\,267\text{J}}{RT}\right), \tag{10}$$

where T_{test} is the absolute test temperature. The regression coefficient was greater than 0.99. The activation energy value associated with DHC in this alloy was 56 267 J/mol, which is slightly lower than that reported in literature (71 500 J) [38]. This activation energy is the sum of the activation energy of hydrogen diffusion (31 617 J [17]) and enthalpy of mixing of hydrogen (38 874 J [17]) in this alloy [38].

5.8. Estimation of life of pressure tube

Pressure tubes in operating reactors operate at a temperature of around 300 °C and under a pressure of 10.5 MPa. This internal pressure results in a hoop stress of the order of 135 MPa. Also, both the ends of the pressure tubes are roll joined to the rest of the primary heat transport circuit. During roll joint formation, the

pressure tube deforms plastically and the end fitting material deforms elastically [5]. Though this ensures a leak tight joint, the ends of the pressure tube are subjected to residual stresses. Thus, under the effect of hoop stress generated due to internal pressure and/or residual stress, there is a possibility that a sub-critical crack may grow to critical size [20] resulting in catastrophic failure of the tube. DHC velocity is required for estimating the time period after which a sub-critical crack will grow to critical size. A simplistic relationship is given in Eq. (11).

$$\mathrm{CCL} = (\text{factor of safety}) \times (a + V_{\mathrm{DHC}}(\text{Life of the component})), \qquad (11)$$

where CCL is the critical crack length under operating stress and a is the crack length determined during the quality control exercise. It should be noted that with an increase in the hydrogen concentration and fluence, the value of critical crack length, CCL decreases. Thus CCL for the pressure tubes depend on the age of the tube.

6. Conclusions

1. The DHC velocity was determined for double melted Zr–2.5Nb pressure tube material along the axial direction of the tube in the temperature range of 162–283 °C. The DHC velocity was found to increase with increase in test temperature.
2. The observed V_{DHC} value was comparable to that previously reported in the literature. The DHC velocity for the double melted Indian material and quadruple melted AECL material are comparable.
3. The DHC velocity is independent of the SIF employed in this investigation. For some tests, an incubation period for crack initiation was observed during DHC testing.
4. The activation energy associated with DHC was found to be nearly equal to the sum of enthalpy of mixing of hydrogen and activation energy for hydrogen diffusion in this alloy.

Note: Part of the work presented in this paper were carried out under IAEA sponsored CRP titled 'Hydrogen and hydride induced degradation of mechanical and physical properties of zirconium alloys' (Research agreement no. 11105).

Acknowledgements

Authors express their deep gratitude to Dr S. Banerjee, Director, Materials Group for his constant encouragement and support for this work. The guidance by Dr P.K. De, Head, Materials Science Division is appreciated. The authors are also thankful to Shri Manjit Singh, Head, Division of Remote Handling and Robotics for making available the autoclaved Zr–2.5Nb PT material for the study on Indian pressure tube material. Authors are grateful to Dr Ian Ritchie of IAEA and his former colleagues from AECL for providing the Zr–2.5Nb alloy CCT specimens and 0.5 mm diameter Zr–2.5Nb wire, which was used in this investigation. The technical assistance provided by Shri N.T. Parekh and Shri P.G. Adiga of Materials Science Division needs special acknowledgement.

References

[1] C.D. Williams, React. Technol. 13 (2) (1970) 147.
[2] E.F. Ibrahim, B.A. Cheadle, Can. Metall. Q 24 (3) (1985) 273.
[3] R.G. Fleck, V. Perovic, E.T.C. Ho, Ontario Hydro Res. Rev. No. (8) (1993) 1.
[4] B.A. Cheadle, C.E. Coleman, H. Litcht, Nucl. Technol. 57 (1982) 413.
[5] D.O. Northwood, U. Kosasih, Int. Met. Rev. 28 (2) (1983) 92.
[6] J.R. Theaker, R. Choubey, G.D. Maon, S.A. Aldridge, L. Davis, R.A. Graham, C.E. Coleman, Zirconium in Nuclear Industry: 10th International Symposium, ASTM-STP-1245 (1994) 221.
[7] R.N. Singh, R. Kishore, T.K. Sinha, BARC Report no. BARC/2001/E/012.
[8] R.N. Singh, R. Kishore, T.K. Sinha, B.P. Kashyap, J. Nucl. Mater. 301 (2002) 153.
[9] C.E. Coleman, AECL-5260 (1976) 1.
[10] L.A. Simpson, K. Nuttall, Zirconium in Nuclear Industry, A.L. Lowe Jr., G.W. Parry (Eds.), American Society of Testing and Materials, ASTM STP 633 (1977) 608.
[11] K.F. Amouzouvi, L.J. Clegg, Metall. Trans. A 18A (1987) 1687.
[12] R.L. Eadie, R.R. Smith, Can. Metall. Q 27 (1988) 213.
[13] B. Cox, J. Nucl. Mater. 170 (1990) 1.
[14] G. Domizzi, R.A. Enrique, J. Ovejero-Gracia, G.C. Buscaglia, J. Nucl. Mater. 229 (1996) 36.
[15] E.G. Price, IAEA Technical Committee Meeting, Mumbai, India, February 1994.
[16] M. Leger, T.P. Byrne, A.C. Wallace, D.V. Leemans, Ontario Hydro Res. Rev. No. (8) (1993) 46.
[17] A. Sawatzky, Can. Metall. Q 24 (3) (1985) 227.
[18] S.S. Kim, S.C. Kwon, Y.S. Kim, J. Nucl. Mater. 273 (1999) 52.
[19] S. Sagat, C.K. Chow, M.P. Puls, C.E. Coleman, J. Nucl. Mater. 279 (2000) 107.
[20] C.E. Coleman, B.A. Cheadle, J.F.R. Ambler, P.C. Lichtenberger, R.L. Eadie, Can. Metall. Q 24 (3) (1985) 245.
[21] R.N. Singh, Niraj Kumar, R. Kishore, S. Roychaudhury, T.K. Sinha, BARC report no. BARC/2001/E/026.
[22] R. Dutton, Metall. Soc. Can. Inst. Metals, Annual Volume, 1978, p. 16.
[23] V. Perovic, G.C. Weatherly, R.G. Fleck, Can. Metall. Q 24 (3) (1985) 253.

[24] D. Srivastava, G.K. Dey, S. Banerjee, Metall. Trans. A 26A (1995) 2707.
[25] R.N. Singh, R. Kishore, S. Roychaudhury, M. Unnikrishnan, T.K. Sinha, P.K. De, S. Banerjee, Santosh Kumar, BARC Report : BARC/2000/E/038.
[26] R.N. Singh, R. Kishore, T.K. Sinha, S. Roychaudhury, P.K. De, S. Banerjee, Report no. BARC.MSD. IAEA.2000.01 on Phase I of IAEA CRP, Presented at 2nd Research Co-ordination Meeting, Pitesti, Romania, 5–9 June 2000.
[27] R. Choubey, FC-IAEA-02, T1.20.13-CAN-27363-02, November 1998.
[28] A.D. Lepage, W.A. Ferris, G.A. Ledoux, FC-IAEA-03, T1.20.13-CAN-27363-03, November 1998.
[29] W. Dietzel, K.-H. Schwalbe, Sonderdruck Materialprufung 28 (11) (1986) 368.
[30] V.A. Markelov, T.N. Zheltkovskaya, V.V. Tsvelev, Russian Report on Phase I of IAEA CRP, Presented at 2nd Research Co-ordination Meeting, Pitesti, Romania, 5–9 June 2000.
[31] R. Choubey, C. Coleman, IAEA-CRP-CAN-27363 Progress Report 1, 1999 presented at 1st Research Co-ordination Meeting, Vienna, Austria, 1999.
[32] Maria Roth Progress Report on Phase I of IAEA CRP, Presented at 2nd Research Co-ordination Meeting, Pitesti, Romania, 5–9 June 2000.
[33] M.P. Puls, AECL Report no. 8381, (1984) 1.
[34] R.W. Hertzberg, in: Deformation and Fracture Mechanics of Engineering Materials, 2nd Ed., Wiley, 1983, p. 154.
[35] Z.L. Pan, I.G. Ritchie, M.P. Puls, J. Nucl. Mater. 228 (1996) 227.
[36] R.L. Edie, C.E. Coleman, Scripta Mater. 23 (1989) 1865.
[37] R.N. Singh, R. Kishore, T.K. Sinha, S. Banerjee, BARC Report no. BARC/2000/E/029.
[38] J.F.R. Ambler, ASTM STP 824, D.G. Franklin, R.B. Adamson, Eds. (1984) 653.